The Journal of Systems and Software 85 (2012) 883–894

Contents lists available at SciVerse ScienceDirect

The Journal of Systems and Software

journal homepage: www.elsevier.com/locate/jss

Intelligent reversible watermarking in integer wavelet domain for medical images

Muhammad Arsalan, Sana Ambreen Malik, Asifullah Khan*

Department of Computer Science, Pakistan Institute of Engineering and Applied Sciences, Nilore-45650, Islamabad, Pakistan

ARTICLE INFO

Article history:
Received 30 September 2010
Received in revised form 28 October 2011
Accepted 1 November 2011
Available online 7 November 2011

Keywords:
Reversible watermarking
Integer wavelet transform (*IWT*)
Histogram recovery
Genetic algorithm (*GA*)
Medical images

ABSTRACT

The prime requirement of reversible watermarking scheme is that the system should be able to restore the cover work to its original state after extracting the hidden information. Reversible watermarking approaches, therefore, have wide applications in medical and defense imagery. In this paper, an intelligent reversible watermarking approach *GA-RevWM* for medical images is proposed. *GA-RevWM* is based on the concept of block-based embedding using genetic algorithm (*GA*) and integer wavelet transform (*IWT*). *GA* based intelligent threshold selection scheme is applied to improve the imperceptibility for a fixed payload or vice versa. The experimental results show that *GA-RevWM* provides significant improvement in terms of imperceptibility for a desired level of payload against the existing approaches.

1. Introduction

In the field of medical science imagery, the protection of medical images as well as their authentic usage is an important issue. Problems in the digital content protection have been emerged due to recent development in the field of multimedia systems and communication technologies. Therefore, security of digital content has gained much more importance and researchers have been developing approaches for protecting and authenticating digital content (Chang and Lin, 2008). Watermarking is one of the prospective solutions to the aforementioned problems (Chang et al., 2009; Pan et al., 2004). It is thus a challenging task to achieve high degree of data security, reliability and authenticity of digital images.

Watermarking approaches, in general, can be classified into robust and fragile watermarking. Robustness is an important property of watermark that enables watermarked image to withstand signal processing operations such as spatial filtering and lossy compression (Khan, 2006; Khan et al., 2004, 2008; Liu and Steinebach, 2006; Lu et al., 2009, 2010). In Tasi et al. (2010), support vector machine (*SVM*) is trained to learn the relationship between watermark and the image-dependent watermark. The trained *SVM* is used to recover the watermark and α-trimmed mean operator makes the system additionally robust against the attacks. In Peng et al. (2010), a wavelet domain based *SVM* watermarking algorithm is presented. Watermark embedding is carried out by modulating the mean value relationship of wavelet coefficients in two approximation subbands. Learning capability of *SVM* is used to learn the mean value relationship and watermark can be correctly extracted at the detector side, even in the presence of different attacks. In Shieh et al. (2004), a genetic algorithm (*GA*) based watermarking scheme is presented. *GA* is used to locate the optimal frequency bands for watermark embedding. In Piva et al. (2005), a simple and secure self-recovery authentication technique is presented, which hides an image digest in subbands of discrete wavelet transform (*DWT*). The technique detects the malicious manipulation by a self-recovery mechanism and possesses robustness against *JPEG* compression.

In case of fragile watermarking, the watermark is destroyed after any processing applied on the content either incidental or malicious. In this regard, discrete cosine transform (*DCT*) and vector quantization based watermarking techniques are proposed to prevent digital content from tampering (Wang et al., 2007). These approaches are able to detect the malicious distortions but they fail against incidental manipulation like *JPEG* compression. Thus semi-fragile watermarking techniques (Chamlawi et al., 2010; Ho and Li, 2004; Peng et al., 2010) have been proposed, which are tolerant against incidental attacks and sensitive to malicious attacks. In Khan et al. (2008), the watermarking approach can accurately authenticate the image but cannot recover it. On the other hand, in Chamlawi et al. (2007), the image is accurately authenticated and can be recovered but at the cost of security and imperceptibility. Fridrich et al. (2001) proposed two techniques for authentication of digital images using invertible watermarking. These techniques introduced a small amount of distortion to the image, which can

* Corresponding author. Tel.: +92 51 2207381; fax: +92 51 2208070.
E-mail addresses: asif@pieas.edu.pk, khan.asifullah@gmail.com (A. Khan).

0164-1212/$ – see front matter © 2011 Elsevier Inc. All rights reserved.
doi:10.1016/j.jss.2011.11.005

be removed completely if the image is authentic. However, these techniques are not being able to authenticate every possible image. Different applications use watermarking approaches according to their requirements. For example, copyright protection based applications need a robust, while authentication based applications need a fragile watermarking system.

In dealing with watermarking of medical images, some important constraints need to be satisfied. When watermark is embedded in the host image, it generates distortion. This distortion is highly undesirable in medical applications, whereby, even a small distortion in the images such as *MRI* and X-ray images might affect the decision of a physician. For this reason, it is necessary not only to extract the watermark but also to restore the original image completely. Reversible watermarking fulfills this requirement. It can restore the exact state of the original image (Chang and Lin, 2008).

An effective way of embedding watermark in the medical image is to define a region of interest (*ROI*). *ROI* is an area, which contains important information and must be stored without any distortion. In Wakatani (2002), a digital watermarking method has been proposed, which avoids the distortion of the image data in *ROI* by embedding information into non-*ROI* regions. Similarly, in Shih and Ta Wu (2005), a robust technique based on *GA* for embedding the watermark around the *ROI* in a medical image, is presented.

Many reversible watermarking techniques have been proposed. Tian (2002) has proposed a high-capacity and high quality reversible watermarking technique, by expanding the pair wise pixel difference. In his work, image is first divided into pair of pixel values. Expandable differences between pair of pixels are selected for expansion and then payload is embedded on it. Alattar (2004) have proposed high capacity reversible data hiding approach by applying the difference expansion to quads of adjacent pixels. Xuan et al. (2006) have presented histogram shifting based reversible watermarking technique. In their work, a part of the histogram of high frequency wavelet coefficients is shifted towards right by one point and then watermark is embedded by using the histogram zero-point. Similarly, Xuan et al. (2002) have proposed reversible data hiding technique in the integer wavelet transformed (*IWT*) domain. This algorithm hides data into one (or more) middle bit-plane(s) of the *IWT* coefficients, in the middle and high frequency subbands. Yang et al. (2004) have published their work on high capacity reversible watermarking. They utilized bit-shift operation for companding process to achieve good imperceptibility and high capacity of watermarked images. Kamstra et al. (2005) have presented a least significant bit (*LSB*) prediction scheme. In this approach, a binary bit stream from the image is extracted first. This bit stream is compressed and then embedded in the image along with the payload by replacing the original bit stream. Similarly, in Tian (2002), the location map besides the watermark is inserted in the image for locating the expanded difference. This generates a significant degradation in the image if there is not enough space left for embedding the location map. Consequently, an efficient tradeoff between capacity and imperceptibility has to be made so that space for the overhead is created. Xuan et al. (2005b) have developed a reversible watermarking application using companding on *IWT* coefficients. Companding is applied by selecting the compression and expansion function to decrease the distortion between original and marked image. Existing reversible watermarking approaches offer effective tradeoff between watermarking capacity and imperceptibility (Kumsawat and Attakitmongcol, 2005; Pan and Abraham, 2009; Tian, 2002; Xuan et al., 2002, 2004, 2005b). This tradeoff is largely dependent on the intelligent selection of threshold, which provides a room for improvement. In this work, we therefore, intend to exploit the learning capabilities of *GA* to develop a threshold matrix for a given image.

A block-based fragile watermarking approach has been proposed, where the threshold for companding in the *IWT* domain is intelligently computed. Xuan et al. (2005b) approach has been followed for the companding operation. The *IWT* domain has been selected as an embedding domain, which improves the reversible property of the watermarking system. This is mainly because the round-off errors are avoided in *IWT*. Additionally, binary GA is considered suitable and easy to implement for an integer value based optimization problem. The block-based embedding helps us in selecting a local optimum threshold for each block through *GA*. For this purpose, we let *GA* exploit information of wavelet coefficients and nature of wavelet subbands to evolve a threshold map *T*. The decision of embedding is taken by using the evolved *T*. The learning capabilities of *GA* make an effective tradeoff between the watermark payload and imperceptibility, which has even more demand in case of medical imagery.

The rest of the paper is organized as follows: The details of proposed algorithm are presented in Section 2. Experimental results and performance analysis are presented in Section 3. Conclusions are drawn in Section 4.

2. Proposed *GA-RevWM* approach

The general architecture of proposed algorithm is based on training and testing phases as shown in Fig. 1. In training phase, *GA* is employed to evolve a matrix *T*, which is utilized in testing phase during embedding and extraction processes.

2.1. Training phase (GA based optimization)

GA is a direct random search technique, inspired by biological evolution, for solving optimization problems. In *GA*, a candidate solution is represented by a data structure called chromosome (in our case it is represented by bit string).

In this work, we have employed *GA* algorithm to generate the optimal threshold matrix *T*, which is required for companding in watermark embedding step. From one generation to the next, *GA* evolves a population consisting of individuals, which are the potential solution for the given problem. Total number of individuals depends upon the parameter population size. Second important parameter of *GA* is number of generations. Each individual of a population is evaluated with the help of fitness function.

In proceeding from one generation to the next, individuals having poor fitness are discarded and new individuals are generated with the help of crossover and mutation operations. These new individuals take the place of the discarded individuals in the next generation (Banzhaf et al., 1998). In order to calculate fitness of an individual, a fitness function is developed in a way to optimize the imperceptibility vs. capacity tradeoff. In the fitness function, after taking *IWT* of an input image, the subbands *HL*, *LH* and *HH* are divided into small blocks. Then watermark is embedded by following the procedure described in Section 2.2.1. Finally, fitness is calculated using watermarked image through mathematical expression shown in Eq. (1).

$$Fitness = \begin{cases} 10 \times \log_{10}\left(\dfrac{255^2}{MSE}\right), & \text{if } effective\_payload \geq desired\_effective\_payload \\ 0, & \text{otherwise} \end{cases} \tag{1}$$

where *effective_payload* is the watermark bits embedded in the image, *desired_effective_payload* is the amount of watermark that we want to embed, and *MSE* represents the mean square error of watermarked image, explained mathematically in Eq. (2):

$$\mathrm{MSE} = \frac{1}{M \times N} \sum_{i=0}^{M-1} \sum_{j=0}^{N-1} [I_O(i,j) - I_W(i,j)]^2 \tag{2}$$

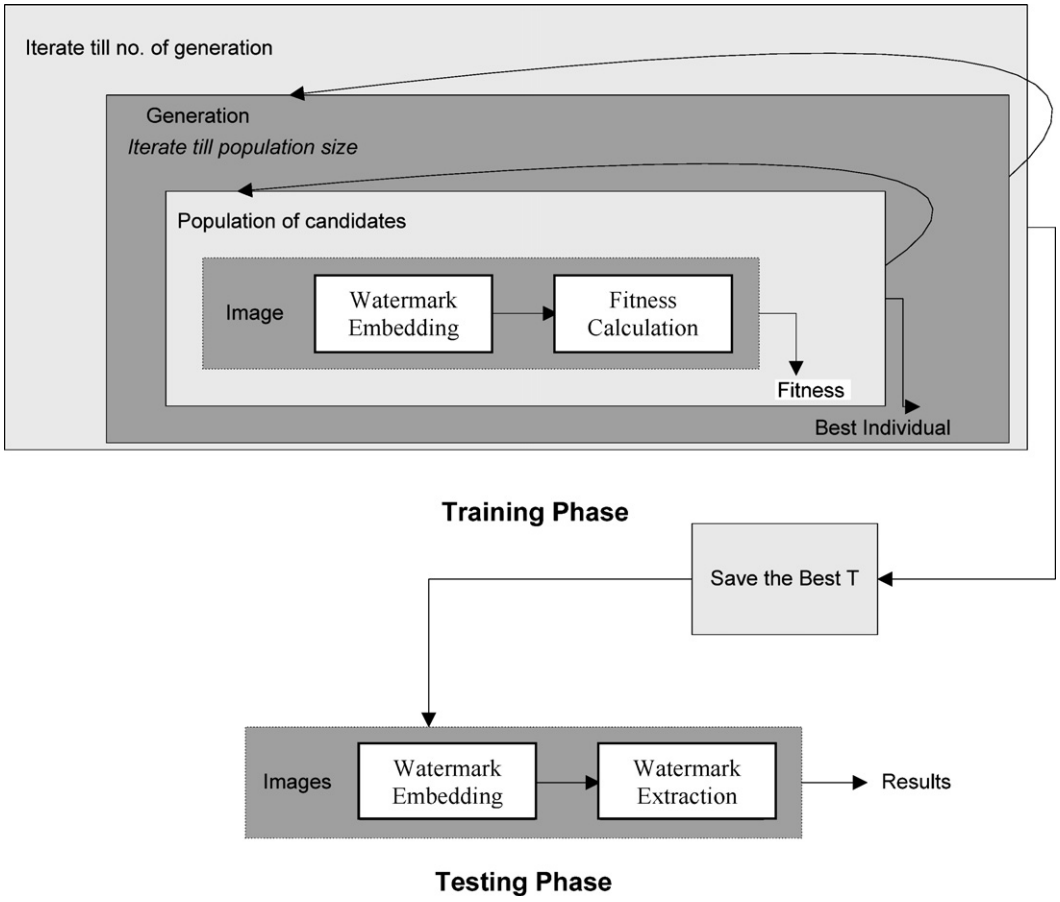

Fig. 1. General architecture of the proposed reversible watermarking algorithm, *GA-RevWM*.

where I_O and I_W are the original and watermarked images, respectively. $M \times N$ represents the size of the image. The individual having high value of fitness is considered as the best individual.

This process continues from generation to generation, by calculating fitness for individuals, until a termination condition is reached. The best threshold matrix represented by T is achieved at the end. This concludes the training phase.

2.2. Testing phase

This phase involves two main processes, embedding and extraction. T (computed in training phase) is used for companding in watermark embedding and for image restoration in watermark extraction processes.

2.2.1. Watermark embedding

The embedding process is shown in Fig. 2. It consists of the following main steps.

2.2.2. Histogram modification

In watermark embedding process, the image is at a risk of underflow and overflow problem. In order to avoid this problem, histogram modification is performed on the image before being used in the watermark embedding stage.

The histogram modification process is explained with the help of an example. Consider an image of size 6×6 with $256 = 2^8$ grayscales as shown in Fig. 3. From this figure, it can be observed that the range of the modified histogram is 1–254 instead of 0–255, i.e. no pixel presume grayscales 0 and 255. After modification, grayscale 1 is merged into grayscale 2 and grayscale 0 converted into grayscale 1. In the same way, grayscale 254 is merged into grayscale 253 and grayscale 255 converted into 254.

In order to reverse the modification in the image histogram at the extraction side, scan sequences are generated. In the modified image, all 1's are because of 0's in the original image and similarly 254's are actually the 255's in the original image. Therefore, we do not need to generate a scan sequence for these two grayscale values. 2's in the modified image are due to the original 2's and the 2's that are obtained after transforming 1's. Similarly, 253's in the modified image are due to the original 253's and the 253's that are obtained after transforming 254's. Therefore, to record this ambiguity scan sequences are generated for grayscale values '2' and '253'.

To generate the scan sequence for grayscale value '2', the original and the histogram-modified images are scanned simultaneously. When the pixel values are '2' at a location (x, y) in both images, '1' is stored in the scan sequence. If histogram modified image contains pixel value '2' and the original image contains pixel value '1' at a location (x, y), '0' is stored in the scan sequence. Length of the sequence is equal to the number of 2's in the histogram-modified image. Similarly, the scan sequence for grayscale 253 is generated (Xuan et al., 2005a).

Next, the bookkeeping data is generated using the generated scan sequence. The bookkeeping data store (say *BDS*) consists of the following information.

$$\begin{aligned} \text{BDS} = [&\text{the total book keeping bit length} \\ &+ \text{compressed number of grayscales} \\ &+ \text{first histogram from left hand side grayscale} \\ &+ \text{record length} + \text{scan sequence} \end{aligned}$$

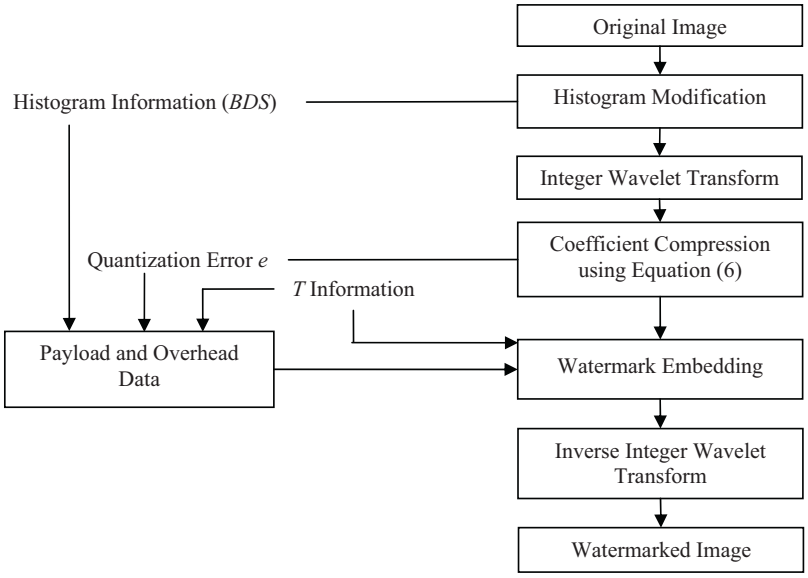

Fig. 2. Block diagram for watermark embedding.

+ the first histogram from right hand side grayscale

+ record length + scan sequence]

From the above discussion, the compressed number of grayscales is two (i.e. '0' and '255'), which may be stored in '4' or '8' bits. First histogram from left hand side grayscale is '1', which can also be stored in 4 or 8 bits. Record length is the length of the scan sequence '2', which is stored in 16 or 32 bits. Then scan sequence '2' is appended. First histogram from right hand side grayscale is '254' and this is stored in appropriate number of bits. Then comes the record length of '253' scan sequence followed by scan sequence '253'. All these are combined to form the *BDS*. *BDS* is stored as overhead in the image and is used at the receiving side to restore the image to its original state as shown in Fig. 2.

2.2.3. Integer wavelet transform

In the next step, *IWT* is applied on the histogram-modified image. It is used for recovering the image without any loss of information. The wavelet family *Cohen-Daubechies-Feauveau* (*CDF*) (2, 2) is used here due to its higher embedding capacity and better visual quality of the marked images (Xuan et al., 2005b). *IWT* is performed to convert the image of size $M \times N$ into wavelet subbands. Four subbands, each of size $M/2 \times N/2$ are shown in Fig. 4. Beginning with upper left corner and moving in a clockwise manner, these quadrants contain approximation subband (*LL*), horizontal detail subband (*LH*), diagonal detail subband (*HH*) and vertical detail subband (*HL*) (Gonzalez and Woods, 2008). *LL* subband is highly sensitive and contains the smooth area of the image. Therefore, small addition of watermark in this subband can cause high perceptual distortion. Thus watermarking is done in the other three subbands.

2.2.4. Data embedding using companding process

Companding is a successive process of compression and expansion. It is mainly used for reducing the data rate of audio signals by selecting unequal quantization levels and hence to achieve high signal to noise ratio. Sklar (1988), in his work, has discussed this technique in detail.

Compression is a process in which a wider range of the signal is mapped to a narrower range and after expansion, we obtain the original signal back. In ideal case (i.e. without digitization), companding operation is described in Eq. (3).

$$f_E(f_C(x)) = x \tag{3}$$

where f_E and f_C are expansion and compression functions, respectively.

(a) Selection of companding function

There are two main purposes of compression. Firstly, the distortion in the original signal after embedding should not be very high so that overflow and underflow could be avoided. Secondly, the marked signal should be close to the original signal so that noise in the signal is minimum.

2	4	255	70	255	98
3	187	5	3	90	1
3	200	255	67	254	243
0	2	2	87	233	234
0	1	3	99	255	233
0	3	177	101	3	2

(a) Original Image data

2	4	254	70	254	98
3	187	5	3	90	2
3	200	254	67	253	243
1	2	2	87	233	234
1	2	3	99	254	233
1	3	177	101	3	2

(a) Modified Image data

Fig. 3. Histogram modification.

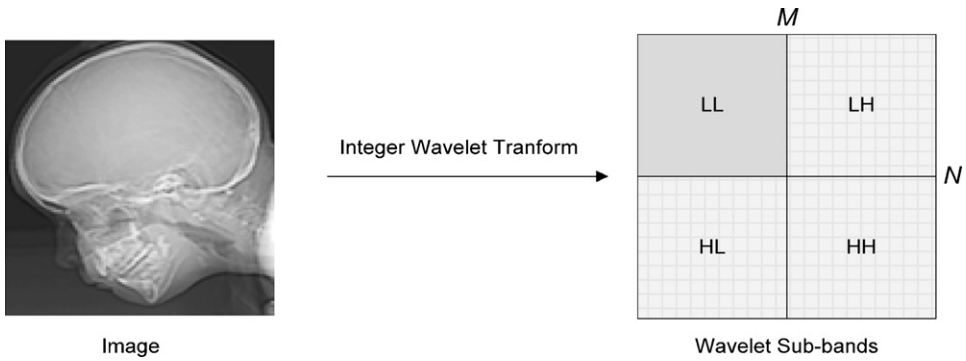

Fig. 4. A subband split of an $M \times N$ image.

In this work, the companding process is similar as employed in Xuan et al.'s approach. However, a slight extension is performed as we are employing block-based embedding. In most of the images, the high frequency coefficients of *IWT* follow Laplacian-like distribution. According to Xuan et al. (2005b), mainly two features exist in the distribution:

- Low valued high frequency *IWT* coefficients do not require any compression due to rare chances of overflow and underflow. Therefore, for these coefficients, it is suitable to use linear compression function with unit slope, i.e. $f(x) = x$.
- High valued high frequency *IWT* coefficients are most likely to cause overflow or underflow after embedding. Therefore, unit slope is no longer appropriate rather a linear compression function with a steep slope is used for them.

In view of the above two situations, a piecewise linear function as the compression function has been used (mathematically shown in Eq. (4)):

$$x_C = f_C(x) = \begin{cases} x, & |x| < T(i,j) \\ sign(x) \cdot \left(\dfrac{|x| - T(i,j)}{2} \right) + T(i,j), & |x| \geq T(i,j) \end{cases} \quad (4)$$

where x_C and x are the compressed and original *IWT* coefficients, respectively. $T(i, j)$ is a threshold value for a particular block (i, j) in which the coefficient x resides. If the total number of blocks in a subband is $m \times n$ (as shown in Fig. 5) then $i = 1, 2, \ldots, m$ and $j = 1,2, \ldots, n$, depending upon the location of x.

For digital signals, Eq. (4) is a poor selection for companding, as it may produces values in the continuous range. Therefore, the quantized version of companding functions; f_{QC} and f_{QE} has to be utilized. Obviously, for some signal x, we may have

$$f_{QE}(f_{QC}(x)) \neq x \quad (5)$$

namely, the error value is $e = f_{QE}(f_{QC}(x)) - x \neq 0$

Hence, in order to recover the original *IWT* coefficient x, we must record the difference value e. The difference value e combined with *BDS* is called overhead data. It is embedded into the host image along with the effective payload (i.e. the watermark). The quantized version of compression and expansion functions are given in Eqs. (6) and (7), respectively.

$$x_C = f_{QC}(x) = \begin{cases} x, & |x| < T(i,j) \\ sign(x) \cdot \left(\left\lfloor \dfrac{|x| - T(i,j)}{2} \right\rfloor + T(i,j) \right), & |x| \geq T(i,j) \end{cases} \quad (6)$$

$$x' = f_{QE}(x_C) = \begin{cases} x_C, & |x_C| < T(i,j) \\ sign(x_C) \cdot (2|x_C| - T(i,j)), & |x_C| \geq T(i,j) \end{cases} \quad (7)$$

Eq. (8) can be applied to recover the original coefficients.

$$x = x' + e \quad (8)$$

(b) Data embedding

After the selection of companding function, the next step is to embed the data. Compression function $f_{QC}(x)$ is applied to the original *IWT* coefficient x to obtain a compressed coefficient i.e. $x_C = f_{QC}(x)$. Assume the binary expression of x_C is $b_1 b_2 \ldots b_n$, where $b_i \in \{0, 1\}$. In the embedding process, a bit $b \in \{0, 1\}$ is appended after the least significant bit (*LSB*) of x_C, which produces $x_{CW} = b_1 b_2 \ldots b_n b$. For example, let $x_C = 4 = (100)_2$ and $b = 1$ then $x_{CW} = (1001)_2 = 9$, it means $x_{CW} = 2 \times x_C + b$. If $f(x) = x$, the variation of the signal after watermark embedding is small and can hardly be perceived.

Selection of suitable value for T is a critical issue. If the value of a coefficient is greater than or equal to T, then it is compressed using the function given in Eq. (6) and a watermark bit is embedded in it otherwise bit is embedded without compression. Smaller value of T significantly reduces the coefficients alteration and hence results in a good visual quality of a marked image. However, corresponding compression error will be larger which will reduce the payload. When T is large, a larger payload is achieved. However, coefficients alteration will be larger and visual quality of the marked image will suffer.

2.3. Watermark extraction and restoration of the original image

On the extraction side, the same procedure is applied as on the embedding side, but in the reverse order. The block diagram of the extraction process is shown in Fig. 6.

2.3.1. Integer wavelet transform

The watermarked image is introduced to watermark extractor on the extraction side. Integer wavelet transform is applied on the marked image to transform it in the wavelet domain.

2.3.2. Data extraction and wavelet coefficient recovery

In watermark extraction stage, the *LSB* bit of signal X_{CW} is extracted, which means $b = LSB(x_{CW})$ and the signal $x_C = (x_{CW} - b)/2$ is obtained. The extracted *LSB* bits contain the original watermark, threshold overhead, companding error overhead and *BDS*. The watermark information and *BDS* is separated from the extracted *LSB* bits. The watermark information is displayed and *BDS* is stored for the next step. After extraction, the signal is still not in its original form because it contains the companding error.

The threshold matrix is obtained from the extracted *LSB* bits and expansion is performed, using Eq. (7). After expansion, extracted

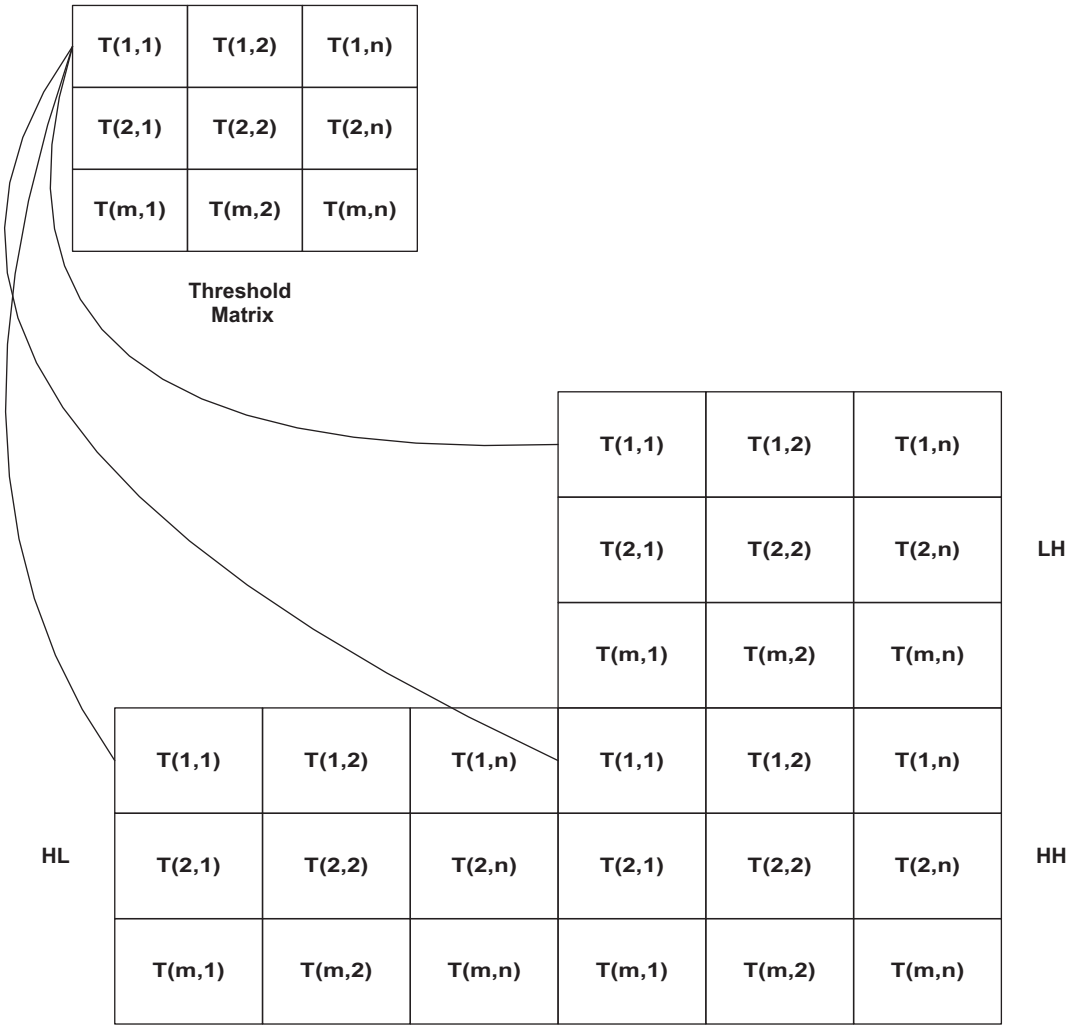

Fig. 5. Mapping of threshold matrix on the blocks of wavelet sub-bands.

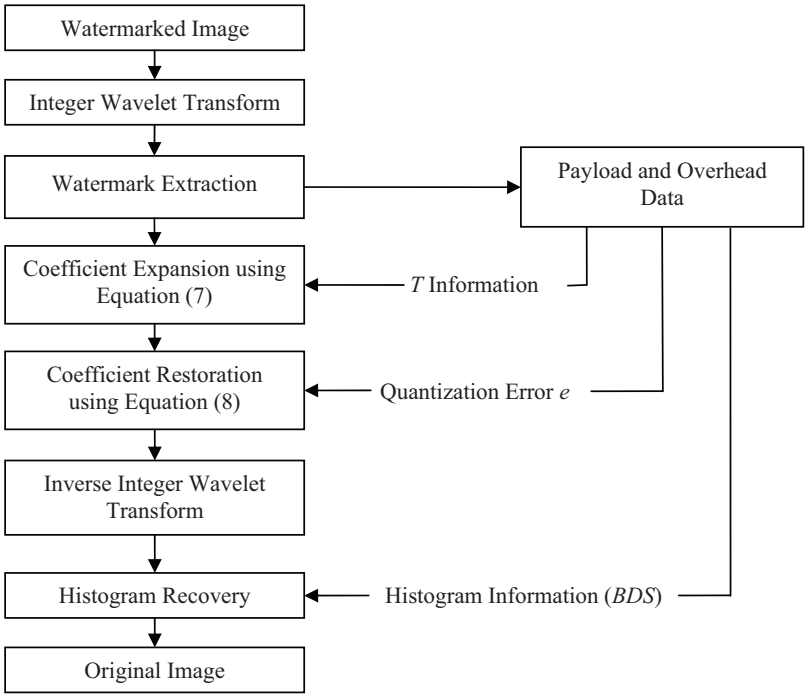

Fig. 6. Block diagram for watermark extraction.

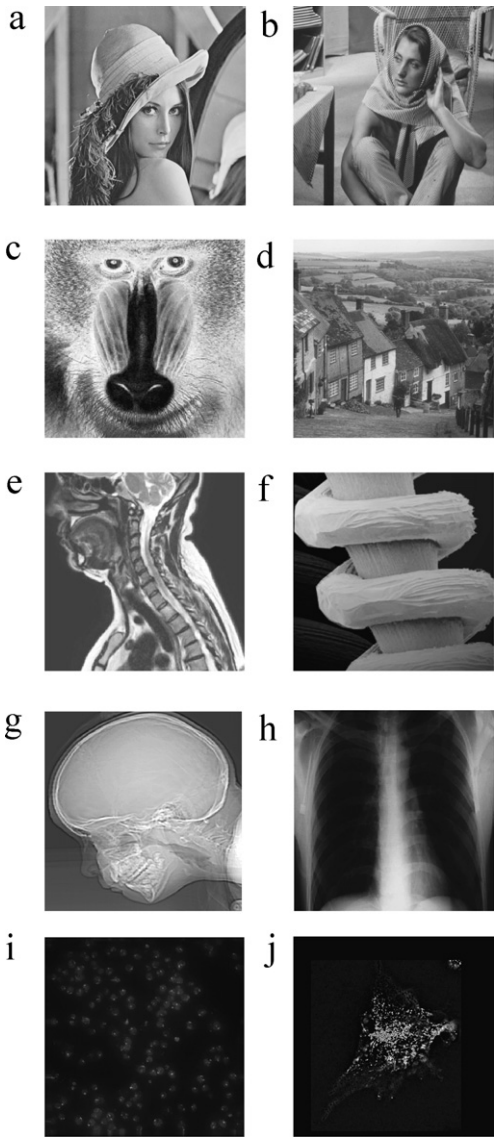

Fig. 7. Images considered for analyzing the performance of proposed *GA-RevWM* technique, (a–d) Standard images, (e–f) MRI images, (g) SEM image (h) X-ray image, (i) Genes image and (j) Cell image.

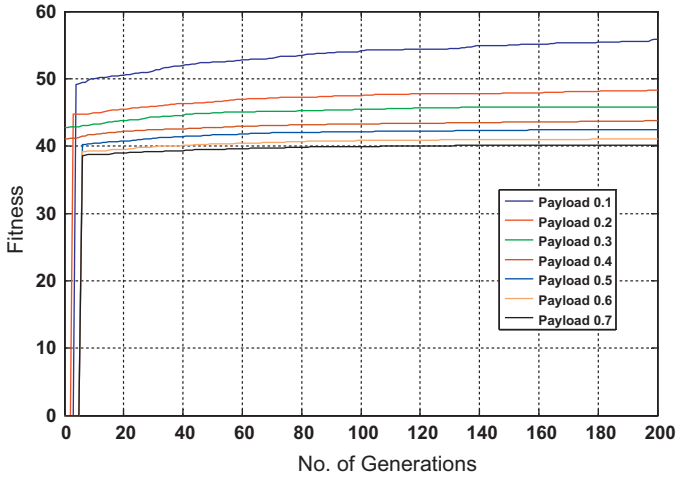

Fig. 8. *GA* simulation for Lena image.

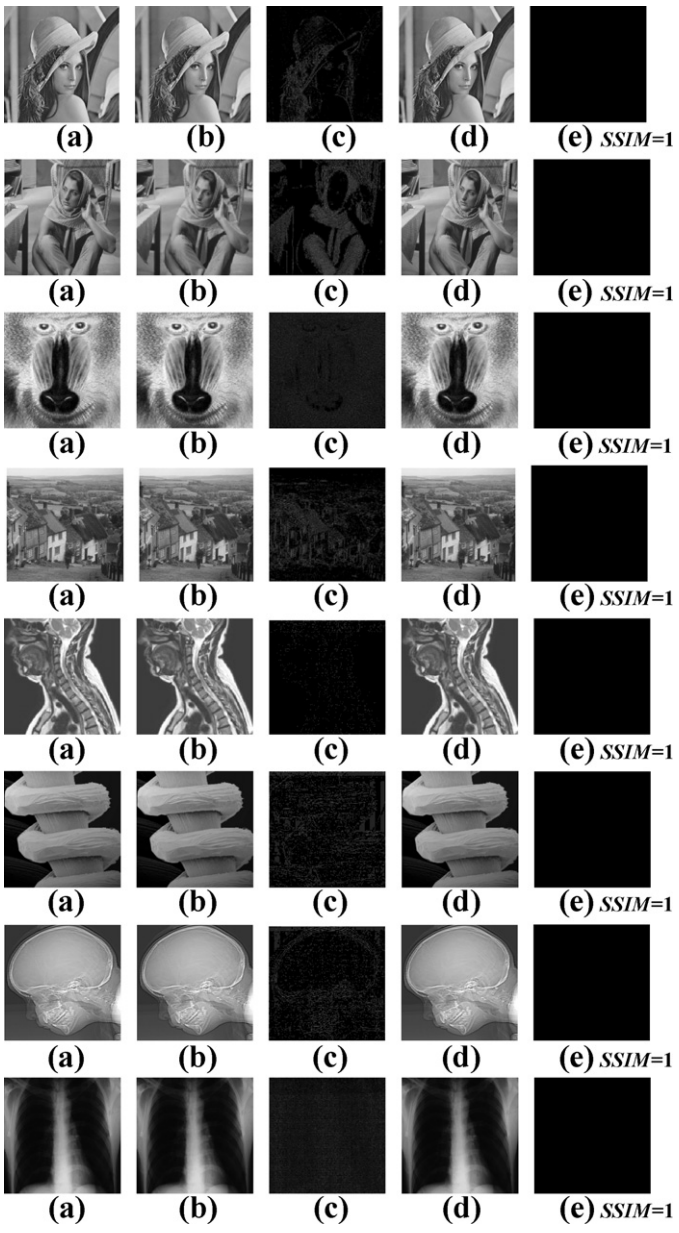

Fig. 9. Column (a) shows original input images, (b) shows the watermarked images, (c) shows the difference between original and watermarked images (difference of (a) and (b)), (d) shows the restored images and (e) shows the difference between original and restored images (difference of (a) and (d)).

error bits are used to recover the original coefficients by applying Eq. (8).

2.3.3. Inverse integer wavelet transform and histogram recovery

After extracting the data and restoring the coefficients to their original state, inverse *IWT* is applied to transform the image back to the spatial domain. Histogram is restored using *BDS*. The scan sequences are used in the same way as described in the histogram modification stage to recover the histogram. Finally, the image attains its original state.

3. Experimental results and discussions

The proposed reversible data hiding technique is applied on some grayscale images shown in Fig. 7. Each of these images is of size 512×512. Number of blocks produces overhead that has a

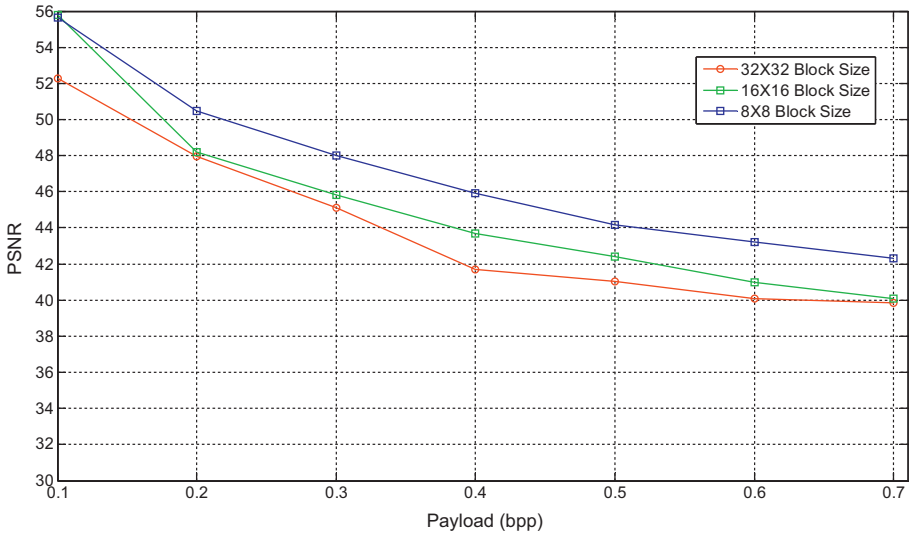

Fig. 10. PSNR vs. payload for block size 8×8 to 32×32 using Lena image.

great effect on the payload, because as the block size increases the size of threshold matrix increases that has to be sent to the extraction side in order to restore the image and watermark. Therefore, the number of blocks should be taken in such a way to achieve good *PSNR* and effective payload. In this paper, block size is taken as 16 thus producing a threshold matrix of size 16×16 ($16 \times 16 = 256$ threshold values).

3.1. GA related implementation details

In order to generate best threshold map, Matlab (Version: R2008b) based *GA* tool has been used. Binary *GA* simulations have been carried out to generate the optimal/near-optimal threshold map by keeping the number of generation 200 and population size 100. In addition, for fitness scaling, rank function has been used that scales the raw scores based on the rank of each individual, rather than its absolute value. The rank of an individual is its position in the sorted scores. Rank fitness scaling removes the effect of the spread of the raw scores. Roulette selection function has been used for choosing parents for the next generation based fitness scaling function. Scattered crossover has been used for combining two individuals to form a new individual, for the next generation. Gaussian mutation is used for providing genetic diversity.

3.2. GA based tradeoff between imperceptibility and capacity

Fig. 8 shows the *GA* simulations that have been carried out for Lena image using different payloads. It can be observed that the value of *PSNR* increases after every generation. Moreover, at the end of the simulation, *GA* produces the optimal/near-optimal threshold map, which gives the best results for a given payload. The zero values in the graph shows those fitness values, which are being discarded. Because for these threshold maps, the companding error is too high that it decreases the effective payload by great amount. So in order to overcome this problem, we give zero fitness to all those threshold maps that do not produce a specified payload (as shown in Eq. (1)). Threshold matrix for Lena image, evolved using *GA* algorithm, is shown in supplementary Table 1 It is to be noted that each threshold of the matrix corresponds to a 16×16 block of the transformed image.

Fig. 9 shows the overall processing of images. It depicts the reversible capability of proposed approach. The column (a) and (b) in Fig. 9 shows the original and watermarked images, respectively. Column (c) shows the difference of the original and watermarked image, demonstrating imperceptible embedding using the best-evolved threshold map. This difference is not visible with naked eye, so an enhancement technique is applied in order to make the difference visible. After extracting the watermark on the extraction side, original contents of the image are retrieved. The resultant restored images are shown in column (d). In order to demonstrate the capability of proposed *GA-RevWM* technique for restoring the original image, the difference of original and restored image is computed. These results are shown in column (e). It is observed that the difference between the original and restored images give us black regions, indicating no difference. In order to see the reversibility performance, *SSIM* (structure similarity measure index) of the original image and restored image is computed. It is observed that all the images, when compared to its restored image, give $SSIM = 1$, which proves the full recovery of the original image.

Fig. 10 shows the effect of changing block size from 8×8 to 32×32. It can be observed that performance is improved with the decrease in block size. As we decrease the block size, the number of coefficients to be handled by *GA* decreases. Therefore, the *GA* has better chances of learning the coefficient distribution and the texture related characteristics associated with that block.

3.3. Performance comparison with existing approaches

Fig. 11 shows the comparison of proposed technique with other existing techniques (Lee et al., 2007; Tian, 2002; Usman and Khan, 2009; Xuan et al., 2002, 2004, 2005b). This comparison is presented in terms of watermark payload and imperceptibility in case of Lena image. It is observed that the proposed scheme achieves better results as compared to other existing techniques. Improvement is due to the learning capability of *GA*, which makes an effective tradeoff between the watermark payload and imperceptibility. Fig. 11 depicts that a payload of 0.7 is achieved against *PSNR* value 40.1 dB, it is a significant improvement provided by the proposed *GA-RevWM* approach. For an image of size 512×512, a payload of 1 means that 262,144 bits are embedded in the image. Since only three subbands are chosen for watermark embedding, therefore, the maximum payload that can be obtained is 0.75. This means that 196,608 bits can be embedded in the image. Fig. 12 shows the variation of *PSNR* against payload for 16-bit images. The effective payload for Gene image is kept 0.6 and for Cell image, it is 0.5.

Through multiple runs of watermark embedding process, we can embed more than 0.75 payload. In Fig. 13, the embedding performance for payload 0–1 in case of Lena image is shown. *SSIM*

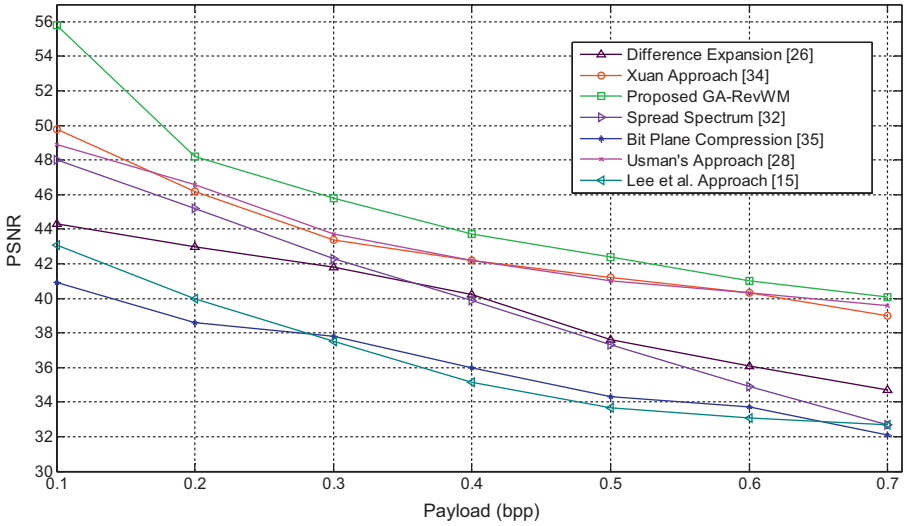

Fig. 11. Performance comparison with existing approaches for Lena image.

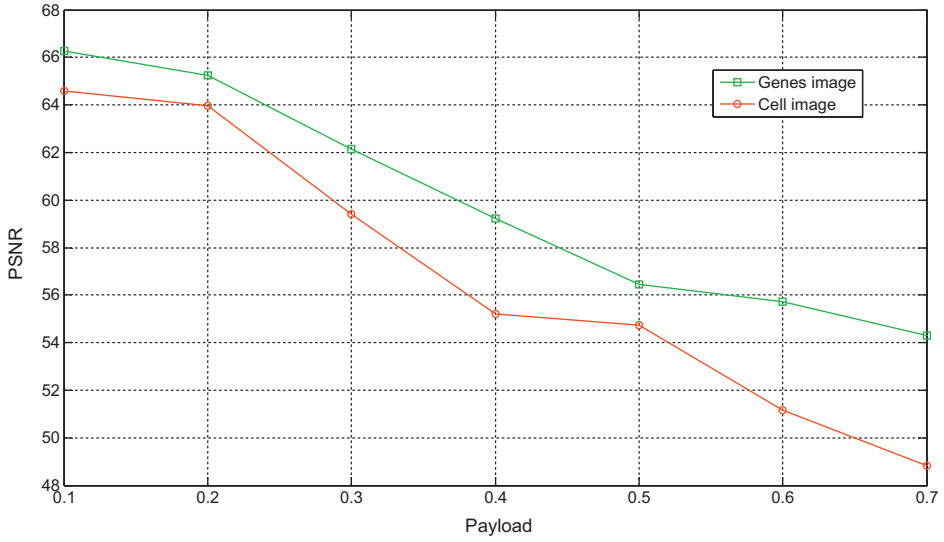

Fig. 12. *PSNR* vs. payload for 16-bit grayscale gene image.

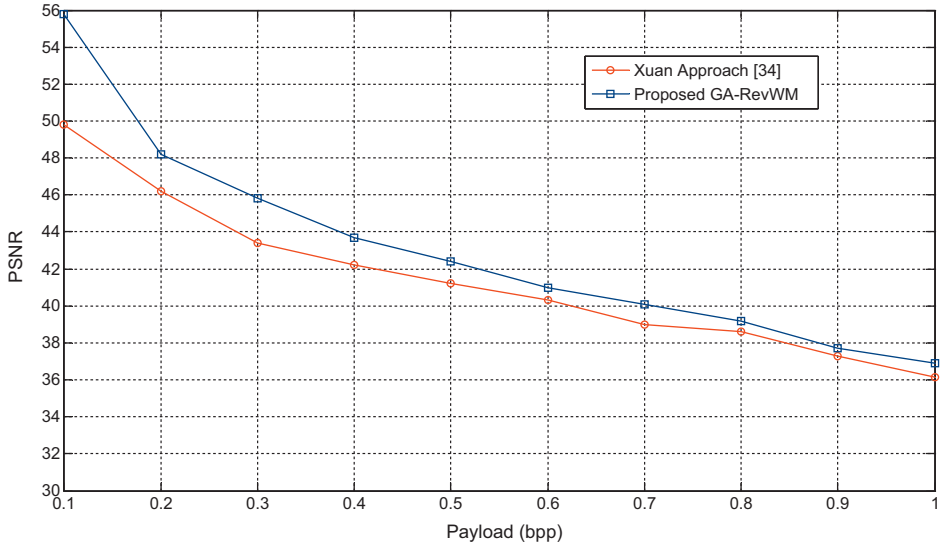

Fig. 13. Performance comparison of proposed *GA-RevWM* approach with Xuan et al. approach (Xuan et al., 2005b) for payload 0–1.

Table 1
Comparison of *PSNR* of proposed *GA-RevWM* technique with that of Xuan et al. (2005b) approach, against different values of payload.

Images	Payload						
	0.1	0.2	0.3	0.4	0.5	0.6	0.7
Lena							
Effect. Payload				0.58			
PSNR (Xuan et al., 2005b)	49.8	46.2	43.4	42.2	41.2	40.3	39.0
PSNR (Proposed *GA-RevWM*)	55.8	48.2	45.8	43.7	42.4	41.0	40.1
Barbra							
Effective Payload				0.48			
PSNR (Xuan et al., 2005b)	48.6	45.6	43.3	41.2	40.6	39.7	38.6
PSNR (Proposed *GA-RevWM*)	55.0	50.9	45.9	44.0	41.1	40.4	39.1
Baboon							
Effect. Payload				0.33			
PSNR (Xuan et al., 2005b)	44.4	41.9	39.9	38.8	38.0	37.2	36.5
PSNR (Proposed *GA-RevWM*)	43.9	47.5	49.3	44.6	42.4	39.1	37.9
Goldhill							
Effect. Payload				0.4			
PSNR (Xuan et al., 2005b)	50.0	46.6	44.4	42.9	41.8	40.9	40.2
PSNR (Proposed *GA-RevWM*)	54.0	51.8	49.2	46.5	43.4	41.7	40.6
MRI1							
Effect. Payload				0.6			
PSNR (Xuan et al., 2005b)	50.2	47.8	45.4	44.0	43.0	42.2	41.5
PSNR (Proposed *GA-RevWM*)	56.2	52.2	48.9	46.7	45.3	44.0	42.8
MRI2							
Effect. Payload				0.6			
PSNR (Xuan et al., 2005b)	52.3	49.7	48.1	46.6	45.2	44.3	43.2
PSNR (Proposed *GA-RevWM*)	56.3	52.2	50.1	48.3	46.5	45.4	44.9
SEM							
Effect. Payload				0.6			
PSNR (Xuan et al., 2005b)	52.4	49.0	47.2	45.5	44.8	44.1	43.5
PSNR (Proposed *GA-RevWM*)	55.9	52.4	49.6	48.1	46.8	45.7	44.9
X-ray							
Effect. Payload				0.6			
PSNR (Xuan et al., 2005b)	53.8	50.0	48.1	46.0	45.6	44.8	44.1
PSNR (Proposed *GA-RevWM*)	56.6	52.7	49.8	48.3	47.1	46.2	44.6

Table 2
Comparison of *SSIM* of proposed *GA-RevWM* technique with that of Xuan et al. (2005b) approach, against different values of payload.

Images	Payload						
	0.1	0.2	0.3	0.4	0.5	0.6	0.7
Lena							
Effect. Payload				0.58			
SSIM (Xuan et al., 2005b)	0.9940	0.9881	0.9826	0.9776	0.9730	0.9682	0.9633
SSIM (Proposed *GA-RevWM*)	0.9982	0.9920	0.9872	0.9807	0.9615	0.9682	0.9625
Barbra							
Effective Payload				0.48			
SSIM (Xuan et al., 2005b)	0.9966	0.9933	0.9896	0.9860	0.9830	0.9793	0.9744
SSIM (Proposed *GA-RevWM*)	0.9988	0.9965	0.9911	0.9890	0.9828	0.9794	0.9726
Baboon							
Effect. Payload				0.33			
SSIM (Xuan et al., 2005b)	0.9979	0.9956	0.9912	0.9864	0.9816	0.9767	0.9723
SSIM (Proposed *GA-RevWM*)	0.9983	0.9981	0.9979	0.9928	0.9867	0.9781	0.9697
Goldhill							
Effect. Payload				0.4			
SSIM (Xuan et al., 2005b)	0.9956	0.9918	0.9886	0.9851	0.9814	0.9786	0.9745
SSIM (Proposed *GA-RevWM*)	0.9983	0.9975	0.9956	0.9919	0.9862	0.9805	0.9730
MRI1							
Effect. Payload				0.6			
SSIM (Xuan et al., 2005b)	0.9976	0.9946	0.9914	0.9883	0.9856	0.9827	0.9799
SSIM (Proposed *GA-RevWM*)	0.9992	0.9977	0.9955	0.9933	0.9910	0.9886	0.9855
MRI2							
Effect. Payload				0.6			
SSIM (Xuan et al., 2005b)	0.9454	0.9443	0.9430	0.9421	0.9404	0.9389	0.9295
SSIM (Proposed *GA-RevWM*)	0.9989	0.9957	0.9928	0.9900	0.9874	0.9846	0.9817
SEM							
Effect. Payload				0.6			
SSIM (Xuan et al., 2005b)	0.9923	0.9889	0.9848	0.9803	0.9762	0.9713	0.9673
SSIM (Proposed *GA-RevWM*)	0.9935	0.9916	0.9870	0.9839	0.9797	0.9751	0.9712
X-ray							
Effect. Payload				0.6			
SSIM (Xuan et al., 2005b)	0.9981	0.9952	0.9917	0.9886	0.9861	0.9833	0.9806
SSIM (Proposed *GA-RevWM*)	0.9993	0.9983	0.9961	0.9939	0.9917	0.9894	0.9862

is another method to measure the image quality/imperceptibility. Therefore, in Fig. 13, results are generated by optimizing *SSIM* for a given payload. The fitness function used to generate these results is shown mathematically in Eq. (9). It can be seen that the proposed technique provides better results even in terms of *SSIM*.

$$Fitness = \begin{cases} SSIM, & \text{if effective\_payload} \geq \text{desired\_effective\_payload} \\ 0, & \text{otherwise} \end{cases} \quad (9)$$

From experiments, the test time taken by the proposed *GA-RevWM* approach and Xuan et al. (2005a) approach has been computed. It has been observed that Xuan et al. approach takes 1.35 s while the proposed *GA-RevWM* takes 0.82 s to watermark Lena image. However, *GA-RevWM* approach consumes more time in training phase; it has taken 45 min to compute optimal/near-optimal threshold. Therefore, in real-world applications, it is better to employ parallel processing based GA simulations for effectively reducing training time.

3.4. Performance comparison on medical images

Tables 1 and 2 present the performance comparison of proposed *GA-RevWM* technique with Xuan et al.'s threshold based companding approach (Xuan et al., 2005b), for different standard and some medical images. Tables 1 and 2 show that the proposed *GA-RevWM* is performing better in terms of *PSNR* and *SSIM* as compared to Xuan et al.'s approach (Xuan et al., 2005b). The results for MRI and X-ray images are obtained by keeping the effective payload greater than 0.6. *GA-RevWM* technique can fully restore the original image and therefore, we do not need to select and avoid *ROI* in medical imagery.

4. Conclusions

In this paper, we have developed an intelligent reversible watermarking approach for medical images. Companding technique is effectively used to achieve higher *PSNR* value for the images and is controlled using threshold. We have observed that the threshold value has a pronounce effect on the actual payload available for watermark embedding. The higher the threshold, the lower is the companding, and the corresponding companding error, and the higher is the *effective payload*. Thus, with change in the threshold, the effective payload and *PSNR* values are also changed but in reciprocating manner.

The learning capability of *GA* is used to make an optimal tradeoff between imperceptibility and payload through effective selection of threshold. This tradeoff has much more importance in case of sensitive imagery such as medical imagery. The characteristics of each wavelet subband are used to evolve a threshold matrix. An optimum threshold value is computed for each of the wavelet subband. The proposed *GA-RevWM* is quite effective and easy to implement. It is capable of providing better imperceptibility for an image at a given effective payload compared to existing reversible watermarking approaches.

Acknowledgments

This work is supported by the Higher Education Commission of Pakistan under the indigenous PhD scholarship programs (106-1555-Eg6-012).

Appendix A. Supplementary data

Supplementary data associated with this article can be found, in the online version, at doi:10.1016/j.jss.2011.11.005.

References

Alattar, A.M., 2004. Reversible watermark using difference expansion of quads. In: Proceedings of IEEE International Conference on Acoustics, Speech and Signal Processing (ICASSP'04), vol. 3, pp. 377–380.
Banzhaf, W., Nordin, P., Keller, E.R., Francone, D.F., 1998. Genetic Programming an Introduction: On the Automatic Evolution of Computer Programs and Its Applications. Morgan Kaufmanns Publishers Inc., San Francisco.
Chamlawi, R., Khan, A., Idris, A., 2007. Wavelet based image authentication and recovery. Journal of Computer Science and Technology 22, 795–804.
Chamlawi, R., Khan, A., Usman, I., 2010. Authentication and recovery of images using multiple watermarks. Journal of Computer and Electrical Engineering 36, 578–584.
Chang, C.C., Lin, P.Y., 2008. Adaptive watermark mechanism for rightful ownership protection. Journal of Systems and Software 81, 1118–1129.
Chang, C.Y., Wang, H.J., Pan, H.J., 2009. A robust DWT-based copyright verification scheme with fuzzy ART. Journal of Systems and Software 82, 1906–1915.
Fridrich, J., Goljan, M., Du, R., 2001. Invertible authentication. In: Proceeding of SPIE Photonics West, Security and Watermarking of Multimedia Contents III, vol. 3971, pp. 197–208.
Gonzalez, R.C., Woods, R.E., 2008. Digital Image Processing, 3rd ed. Dorling Kinderslay, Delhi.
Ho, C.K., Li, C., 2004. Semi-fragile watermarking scheme for authentication of JPEG images. In: International Conference on Information Technology, Coding and Computing (ITCC'04), pp. 7–11.
Kamstra, et al., 2005. Reversible data embedding into images using wavelet techniques and sorting. IEEE Transaction on Image Processing 14 (12), 2082–2090.
Khan, A., 2006. Intelligent perceptual shaping of a digital watermark. PhD thesis, Faculty of Computer Science, GIK Institute, Pakistan.
Khan, A., Mirza, A.M., Majid, A.M., 2004. Optimizing perceptual shaping of a digital watermark using genetic programming. Iranian Journal of Electrical and Computer Engineering 3, 144–150.
Khan, A., Tahir, S.F., Majid, A., Choi, T.S., 2008. Machine learning based adaptive watermark decoding in view of an anticipated attack. Journal of Pattern Recognition, Elsevier Science 41, 2594–2610.
Kumsawat, P., Attakitmongcol, K., 2005. A new approach for optimization in image watermarking by using genetic algorithms. IEEE Transaction on Signal Processing 53 (12), 4707–4719.
Lee, et al., 2007. Reversible image watermarking based on integer-to-integer wavelet transform. IEEE Transaction on Information Forensics and Security 2 (3), 321–330.
Liu, H., Steinebach, M.,2006. Semi-fragile watermarking for image authentication with high tampering localization capability. In: Proceeding of the 2nd International Conference on Automated Production of Cross Media Content for Multi-Channel Distribution. IEEE, pp. 143–152.
Lu, W., Sun, W., Lu, H., 2009. Robust watermarking based on DWT and nonnegative matrix factorization. Journal of Computer and Electrical Engineering 35, 183–188.
Lu, W., Lu, H., Chung, F., 2010. Feature based robust watermarking using image normalization. Journal of Computer and Electrical Engineering 36, 2–18.
Pan, J.S., Abraham, A. (Eds.), 2009. Bio-inspired Information Hiding: A Fusion of Foundations, Methodologies and Applications, vol. 13, issue no. 4. Springer.
Pan, J.S., Huang, H.C., Jain, L.C. (Eds.), 2004. Intelligent Watermarking Techniques. World Scientific, Singapore.
Peng, H., Wang, J., Wang, W., 2010. Image watermarking method in multiwavelet domain based on support vector machines. Journal of Systems and Software 83, 1470–1477.
Piva, A., Bartolini, F., Caldelliy, R., 2005. Self-recovery authentication of images in the DWT domain. Journal of Image and Graphics 5 (1), 149–165.
Shieh, C.-S., Huang, H.-C., Wang, F.-H., Pan, J.-S., 2004. Genetic watermarking based on transform domain techniques. Pattern Recognition 37, 555–565.
Shih, F.Y., Ta Wu, Y., 2005. Robust watermarking and compression for medical images based on genetic algorithms. Journal of Information Sciences 175 (3), 200–216.
Sklar, B., 1988. Digital Communications: Fundamentals and Applications. Englewood Cliffs, New Jersey.
Tasi, H.H., Tseng, H.C., Lai, S.Y., 2010. Robust lossless image watermarking based on α-trimmed mean algorithm and support vector machine. Journal of Systems and Software 83, 1015–1028.
Tian, J., 2002. Reversible watermarking by difference expansion. In: Proceedings of Workshop on Multimedia and Security, pp. 19–22.
Usman, I., Khan, A., 2009. Reversible watermarking based on intelligent coefficient selection and integer wavelet transform. Journal of Innovative Computing, Information and Control 5, 4675–4682.
Wakatani, A., 2002. Digital watermarking for *ROI* medical images by using compressed signature image. In: 35th Annual Hawaii International Conference on System Sciences (HICSS-35'02), pp. 2043–2048.
Wang, F., Yen, K.K., Jain, L.C., Pan, J., 2007. Multiuser-based shadow watermark extraction system. Journal of Information Sciences, Elsevier Science 177 (12), 2522–2532.
Xuan, G., Zhu, J., Chen, J., Shi, Y.Q., Shi, Y.Q., Ni, Z., Su, W., 2002. Distortionless data hiding based on integer wavelet transform. IEEE Electronics Letters 38 (25), 1646–1648.

Xuan, G., Shi, Y.Q., Ni, Z., 2004. Reversible data hiding based on wavelet spread spectrum. In: IEEE International Workshop on Multimedia Signal Processing, pp. 211–214.
Xuan, G., Shi, Y.Q., Yang, C., Zou, D., Chai, P., 2005a. Lossless data hiding using integer wavelet transform and threshold embedding technique. In: Proceedings of the 2005 IEEE International Conference on Multimedia and Expo, pp. 1520–1523.
Xuan, G., Yang, C., Zhen, Y., Shi, Y.Q., Ni, Z., 2005b. Reversible data hiding using integer wavelet transform and companding technique. Lecture Notes in Computer Science 3304, 115–124.
Xuan, G., Yao, Q., Yang, C., Gao, J., Chai, P., Shi, Y.Q., Ni, Z., 2006. Lossless data hiding using histogram shifting method based on integer wavelet. In: International Workshop on Digital Watermarking, vol. 4283, pp. 323–332.
Yang, B., Schmucker, M., Funk, W., Busch, C., Sun, S., 2004. Integer DCT-based reversible watermarking for images using companding technique. In: Proceedings of SPIE, vol. 5306, pp. 405–415.

Muhammad Arsalan received his Bachelor degree in Computer and Information Sciences from Pakistan Institute of Engineering and Applied Sciences (PIEAS), Islamabad, Pakistan, in 2010. He is currently doing M.S. in Computational Engineering in University of Rostock, Rostock, Germany. His research areas include Watermarking, Image Processing, Compressive Sensing, and Evolutionary Algorithms.

Sana Ambreen Malik received her M.Sc. degree in Computer Sciences from Quaid-i-Azam University Islamabad, Pakistan in 2005 and her M.S. degree in Systems Engineering from Pakistan Institute of Engineering and Applied Sciences (PIEAS), Islamabad, Pakistan, in 2007. She is currently doing Ph.D. from Pakistan Institute of Engineering and Applied Sciences (PIEAS), Islamabad, Pakistan. Her research areas include Digital Watermarking, Image Processing, and Evolutionary Algorithms.

Asifullah Khan received his M.Sc. degree in Physics from University of Peshawar, Pakistan in 1996 and his M.S. degree in Nuclear Engineering from Pakistan Institute of Engineering and Applied Sciences (PIEAS), Islamabad, Pakistan, in 1998. He received his M.S. and Ph.D. degrees in Computer Systems Engineering from Ghulam Ishaq Khan Institute of Engineering Sciences and Technology (GIK Institute), Topi, Pakistan, in 2003 and 2006, respectively. He has carried out two-years Post-Doc Research at Signal and Image Processing Lab, Department of Mechatronics, Gwangju Institute of Science and Technology, South Korea. He has more than 14 years of research experience and is working as Associate Professor in Department of Computer and Information Sciences at PIEAS. His research areas include Digital Watermarking, Pattern Recognition, Image Processing, Evolutionary Algorithms, Bioinformatics, Machine Learning, and Computational Materials Science.